Robust quantum optimal control for Markovian quantum systems

Ran Liu,[1] Xiaodong Yang,[1,2,*] and Jun Li[1,2,†]

[1]*Institute of Quantum Precision Measurement, State Key Laboratory of Radio Frequency Heterogeneous Integration, College of Physics and Optoelectronic Engineering, Shenzhen University, Shenzhen 518060, China*

[2]*Quantum Science Center of Guangdong-Hong Kong-Macao Greater Bay Area (Guangdong), Shenzhen 518045, China*

(Received 5 March 2024; accepted 18 June 2024; published 1 July 2024)

Resisting diverse noise effects is crucial for the accurate manipulation of quantum systems. For static or slowly varying noises, many efficient noise mitigation strategies have been developed, such as composite pulses and dynamical decoupling. However, for fast fluctuating noise in the Markovian limit, whether and to what extent coherent quantum control can enhance quantum engineering tasks remains unclear and less explored. Here, we propose a robust quantum optimal control method to tackle Markovian noises. The basic idea is that, regarding the Markovian noise channel as perturbation, we quantitatively characterize the noise-induced error evolution by the perturbative expansion term, and then take them as the objective functions to be suppressed. During optimization, the optimal controls are obtained by maximizing the control target function and meanwhile minimizing the perturbative terms due to Markovian noise order by order. As demonstration examples, we first apply our method to quantum state transfer tasks on two-level and three-level Λ systems, then use it to design quantum gates in two-level and three-level ladder systems, all under Markovian noises. The simulation results illustrate that our method can notably enhance quantum state transfer fidelities and have very limited improvement on gate fidelities. The method presented here is versatile and can be extended to enhance the performance of various control tasks under Markovian noise in multilevel or multiqubit quantum systems.

DOI: 10.1103/PhysRevA.110.012402

I. INTRODUCTION

Precisely manipulating quantum systems is essential for the realization of various quantum technologies [1]. However, quantum systems are fragile and easily affected by a variety of noises. Over the past several decades, numerous effective methods, such as composite pulses [2–4] and robust quantum control [5–8], have been successfully demonstrated to enhance control performance, typically operating under the assumption that the considered noise is quasistatic. This assumption is not universally valid, as noise can undergo temporal changes in many quantum systems [9]. To date, tremendous experiments have unveiled time-correlated features of noises across various qubit platforms, including superconducting circuits [10,11], spin defects [12,13], and ion traps [14,15]. For slowly varying noises, there also have existed several notable suppression techniques, including dynamical decoupling [16–18] and methods under the filter function formalism [19–21]. On the contrary, for fast varying noises, the investigation into how quantum control can enhance the performance of typical engineering tasks, and to what extent, represents a less-explored area.

Resisting fast fluctuating noise is usually highly challenging due to its distinct features. Typically, the correlation time of fast fluctuating noise is much shorter than the timescale of system dynamics; hence, the Markovian approximation is applicable [22]. In this scenario, the system dynamics can be effectively described by the Lindblad equation [23,24]. However, the memoryless nature of Markovian systems makes it challenging to recover information leaked into the environment [25]. This implies that coherent controls cannot easily undo the Markovian noise effects [26], as observed in the static or slowly varying case. Extensive research efforts have aimed to mitigate Markovian noise through quantum optimal control [27–31]. While this approach offers flexibility in addressing various control targets and constraints, the achieved improvements are often limited and come at the expense of significant computational resources. Quantum error correction is routinely designed to mitigate the impact of Markovian noise, yet it requires a substantial number of physical qubits and additional extensive quantum operations below the precision threshold [32–34]. Another commonly employed technique for mitigating Markovian noise involves decoherence-free subspaces [35–37], provided that the system-bath interaction exhibits a symmetry, but a suitable symmetry is not always present. Additionally, the controllability and reachable sets for Markovian systems are not fully understood [38–41]. Hence, there is an ongoing need to develop practical control methods to resist Markovian noises.

In this work, we introduce a robust quantum optimal control method specifically designed to address Markovian noise in common quantum control tasks. The crucial distinction from conventional quantum optimal control methods lies in the incorporation of robustness to the considered Markovian noise into the control target function. This robustness is

*Contact author: yangxd@szu.edu.cn
†Contact author: lijunquantum@szu.edu.cn

effectively quantified by employing the concept of directional derivatives introduced in Ref. [42], which measures the variation in the time-evolution operator due to noise perturbation. Moreover, these directional derivatives can be conveniently calculated using the Van Loan integral formula [43]. Together with the primary control target, such as quantum state or gate fidelity, we address this multiobjective optimization problem using the widely employed gradient ascent pulse engineering (GRAPE) algorithm [44]. As a demonstration, we assess the performance of the proposed robust quantum optimal control method in quantum state transfer and quantum gate preparation tasks under Markovian noise for both two-level and three-level systems. In particular, for state transfer in a three-level Λ system, we compare our method with the conventional stimulated Raman adiabatic passage (STIRAP) pulses [45]. Additionally, for gate preparation in a three-level ladder system, our method is compared with the conventional GRAPE algorithm, both starting from the derivative removal by adiabatic gate (DRAG) pulse [46]. The numerical simulations indicate that our method can significantly improve the performance of quantum state transfer in the presence of Markovian noise, while having little impact on gate fidelity. The underlying reason can be explained as follows: It is comparatively easier to find a specific robust evolutionary trajectory for state transfer than to maintain robustness across the entire space for a quantum gate, as the latter involves more constraints. The proposed method presented here is general and can be readily extended to address Markovian noises in other control tasks or in multiqubit and multilevel quantum systems.

II. METHODOLOGY

We consider the task of designing robust controls to mitigate the Markovian noise effects in common control scenarios. In the following, we introduce our robust quantum optimal control method.

A. Description of Markovian dynamics

In many quantum systems, the interacting environments can be assumed to be large and memoryless, thereby validating the use of Markovian approximation [47,48]. The dynamics of a Markovian quantum system can be described by the master equation in Lindblad form [23], i.e.,

$$\dot{\rho} = -i[H(t), \rho] + \hat{\mathcal{R}}\rho, \tag{1}$$

where ρ is the system density matrix, $H(t)$ represents the noiseless Hamiltonian, $\hat{\mathcal{R}}$ is the dissipative superoperator that characterizes the Markovian noises, and $[A, B] = AB - BA$ denotes the commutator. Precisely, the superoperator $\hat{\mathcal{R}}$ has a general form

$$\hat{\mathcal{R}}\rho = \sum_{\alpha} \Gamma_{\alpha}\left(L_{\alpha}\rho L_{\alpha}^{\dagger} - \frac{1}{2}\{L_{\alpha}^{\dagger}L_{\alpha}, \rho\}\right), \tag{2}$$

where the subscript α signifies the αth noise channel, L_{α} is the Lindblad operator modeling the effect of the αth noise, Γ_{α} is the corresponding dissipative rate, and $\{A, B\} = AB + BA$ is the anticommutator. Under control, the noiseless Hamiltonian can generally be written as $H(t) = H_S + \sum_l u_l(t)H_C^l$, where H_S and H_C^l are the system Hamiltonian and the lth control Hamiltonian, respectively, and $u_l(t)$ is the corresponding control amplitude with respect to H_C^l.

For the sake of convenience, we move to the Bloch vector representation [40,49] by introducing an orthogonal and complete basis set $\mathcal{B} = \{B_k\}_{k=0}^{N^2-1}$, where $\mathrm{Tr}(B_k B_j)/N = \delta_{kj}$, $k, j = 0, \ldots, N^2 - 1$ with N the system dimension. For example, the basis set for two-level systems can be formed through the products of the Pauli matrices, and for three-level systems, it can be derived from the Gell-Mann matrices. Then, we can rewrite Eq. (1) as

$$\dot{\mathbf{r}} = \left(\mathbf{H}(t) + \sum_{\alpha} \Gamma_{\alpha}\mathbf{L}^{\alpha}\right)\mathbf{r}, \tag{3}$$

where $\mathbf{r} = (r_0, \ldots, r_k, \ldots, r_{N^2-1})^{\mathrm{T}}$ represents the state vector with $r_k = \mathrm{Tr}(\rho B_k)/N$, and the elements of $\mathbf{H}(t)$ and $\mathbf{L}^{\alpha}$ can be expressed as

$$\mathbf{H}_{kj} = \mathrm{Tr}(iH(t)[B_k, B_j]), \tag{4}$$

$$\mathbf{L}_{kj}^{\alpha} = \mathrm{Tr}(L_{\alpha}^{\dagger}B_k L_{\alpha} B_j) - \tfrac{1}{2}\mathrm{Tr}(L_{\alpha}^{\dagger}L_{\alpha}\{B_k, B_j\}). \tag{5}$$

The solution of the linear matrix differential equation in Eq. (3) can then be formulated as the following form

$$\mathbf{r}(t) = \mathcal{T}\exp\left(\int_0^t dt_1[\mathbf{H}(t_1) + \sum_{\alpha}\Gamma_{\alpha}\mathbf{L}^{\alpha}]\right)\mathbf{r}(0), \tag{6}$$

where $\mathcal{T}$ is the time-ordering operator. In this way, we can more easily calculate the controlled system's dynamic evolution under Markovian noise determined by the dissipative terms $\{\mathbf{L}^{\alpha}\}$.

B. Perturbative analysis of Markovian noise

As described in Eq. (6), the total time-evolution operator can be written as

$$V(t) = \mathcal{T}\exp\left(\int_0^t dt_1[\mathbf{H}(t_1) + \sum_{\alpha}\Gamma_{\alpha}\mathbf{L}^{\alpha}]\right). \tag{7}$$

To conveniently analyze the Markovian noise effects, we first move to the toggling frame, where the frame transformation operator is defined as

$$V_{\mathrm{tog}}(t) = \mathcal{T}\exp\left(\int_0^t dt_1 \sum_{\alpha}\Gamma_{\alpha}\widetilde{\mathbf{L}}^{\alpha}(t_1)\right). \tag{8}$$

Here, $\widetilde{\mathbf{L}}^{\alpha}(t) \equiv U^{\dagger}(t)\mathbf{L}^{\alpha}U(t)$, and $U(t)$ is the noiseless evolution, i.e.,

$$U(t) = \mathcal{T}\exp\left(\int_0^t dt_1\mathbf{H}(t_1)\right). \tag{9}$$

Based on these definitions, it holds that

$$V(t) = U(t)V_{\mathrm{tog}}(t), \tag{10}$$

which means that the noise effects can be separated out from the overall evolution. We remind that all these operators are N^2-dimensional matrices. Subsequently, we assume that Γ_α is small, thus the total evolution operator $V(t)$ can be perturbatively expanded using the Dyson series [50], i.e.,

$$V(t) = U(t)\left(\mathbb{1} + \sum_\alpha \int_0^t dt_1 \Gamma_\alpha \widetilde{\mathbf{L}}^\alpha(t_1) + \sum_{\alpha,\beta} \int_0^t dt_1 \int_0^{t_1} dt_2 \Gamma_\alpha \Gamma_\beta \widetilde{\mathbf{L}}^\alpha(t_1)\widetilde{\mathbf{L}}^\beta(t_2) + \cdots\right).$$

In general, the noise effects can be alleviated by systematically reducing these perturbative terms, order by order. Several studies have been dedicated to mitigating the noise effects by analytically minimizing the lower orders of the perturbative terms [6,51]. Nevertheless, handling higher-order perturbations and multiple types of noises becomes challenging due to the increased complexity involved in the analysis.

To efficiently quantify and minimize the perturbative terms, we adopt the concept of directional derivatives [42], which are defined as the derivatives of $V(t)$ with respect to Γ_α at $\Gamma_\alpha = 0$. For example, the first-order and the second-order directional derivatives can be defined as

$$D_U^{(1)}(\mathbf{L}^\alpha) \equiv \left.\frac{dV(t)}{d\Gamma_\alpha}\right|_{\Gamma_\alpha=0} = U(t)\int_0^t dt_1 \widetilde{\mathbf{L}}^\alpha(t_1) \tag{11}$$

and

$$D_U^{(2)}(\mathbf{L}^\alpha, \mathbf{L}^\beta) \equiv \left.\frac{d^2V(t)}{d\Gamma_\alpha d\Gamma_\beta}\right|_{\Gamma_\alpha=\Gamma_\beta=0} = 2U(t)\int_0^t dt_1 \int_0^{t_1} dt_2 \widetilde{\mathbf{L}}^\alpha(t_1)\widetilde{\mathbf{L}}^\beta(t_2), \tag{12}$$

respectively. The higher-order directional derivatives can be derived in a similar way. Now, we can easily quantify the deviation of a system's evolution from its ideal trajectory caused by the presence of noise. However, it is resource-consuming to directly calculate the multiple-fold integral in the above expressions of the directional derivatives. Fortunately, as Ref. [42] pointed out, this issue can be effectively addressed by constructing the following Van Loan differential equation [43]

$$\dot{\mathcal{V}}(t) = \mathcal{G}(t)\mathcal{V}(t), \quad \mathcal{V}(0) = \mathbb{1}, \tag{13}$$

where $\mathcal{G}(t)$ represents a block matrix comprising n types of Markovian noises described by the dissipative operators $\mathbf{L}^\alpha, \mathbf{L}^\beta, \ldots, \mathbf{L}^\gamma$, i.e.,

$$\mathcal{G}(t) = \begin{pmatrix} \mathbf{H}(t) & \mathbf{L}^\alpha & 0 & \ldots & 0 \\ 0 & \mathbf{H}(t) & \mathbf{L}^\beta & \ldots & 0 \\ \vdots & \vdots & \vdots & \ddots & \vdots \\ 0 & 0 & 0 & \ldots & \mathbf{L}^\gamma \\ 0 & 0 & 0 & \ldots & \mathbf{H}(t) \end{pmatrix}. \tag{14}$$

According to the Van Loan integral formula [42,43], the solution of Eq. (13) can be expressed as

$$\mathcal{V}(t) = \mathcal{T}\exp\left(\int_0^t \mathcal{G}(t_1)dt\right) = \begin{pmatrix} U(t) & D_U^{(1)}(\mathbf{L}^\alpha)(t) & D_U^{(2)}(\mathbf{L}^\alpha, \mathbf{L}^\beta)(t) & \ldots & D_U^{(n)}(\mathbf{L}^\alpha, \mathbf{L}^\beta \ldots, \mathbf{L}^\gamma)(t) \\ 0 & U(t) & D_U^{(1)}(\mathbf{L}^\beta)(t) & \ldots & D_U^{(n-1)}(\mathbf{L}^\beta, \ldots, \mathbf{L}^\gamma)(t) \\ \vdots & \vdots & \ddots & & \vdots \\ 0 & 0 & 0 & \ldots & D_U^{(1)}(\mathbf{L}^\gamma)(t) \\ 0 & 0 & 0 & \ldots & U(t) \end{pmatrix}. \tag{15}$$

As such, we can conveniently extract the directional derivatives from the off-diagonal elements of $\mathcal{V}(t)$ shown in Eq. (15).

C. Procedure of the robust quantum optimal control

Now we can minimize the directional derivatives to reduce the noise effects with the help of robust optimal control. We first specify a primary target function $f_0(u)$ for the control task of consideration, such as quantum state or gate preparation. For example, Let $U(T)$ denote the noise free time-evolution operator at the final time $t = T$, the state fidelity in the Bloch representation can be expressed as

$$f_{0,\text{state}}(u) = N\mathbf{r}_{\text{tar}}^{\text{T}} U(T)\mathbf{r}(0), \tag{16}$$

where $\mathbf{r}_{\text{tar}}$ represents the target state vector, the superscript "T" denotes the transpose operation. The average gate fidelity is defined as

$$f_{0,\text{gate}}(u) = \frac{\sum_j (U_{\text{tar}}\mathbf{v}_j)^{\text{T}} U(T)\mathbf{v}_j + N^2}{N^2(N+1)}, \tag{17}$$

where $\mathbf{v}_j/\sqrt{N}$ forms an orthonormal operator basis for an N-dimensional system in the Bloch representation [52]. $f_{0,\text{gate}}$ can be simplified as

$$f_{0,\text{gate}}(u) = \frac{1}{3}\sum_{j=\pm x,\pm y,\pm z} (U_{\text{tar}}\mathbf{r}_j)^{\text{T}} U(T)\mathbf{r}_j, \tag{18}$$

where $\mathbf{r}_{\pm x} = [\frac{1}{2}, \pm\frac{1}{2}, 0, 0]^{\text{T}}$, $\mathbf{r}_{\pm y} = [\frac{1}{2}, 0, \pm\frac{1}{2}, 0]^{\text{T}}$, and $\mathbf{r}_{\pm z} = [\frac{1}{2}, 0, 0, \pm\frac{1}{2}]^{\text{T}}$ are six axial states on the Bloch sphere [53], and U_{tar} is the target gate in the Bloch representation. This expression can also be extended to the average gate fidelity of two-dimensional subspace in a three-level system [46]. We then define an additional cost function to assess the magnitude of directional derivatives, aimed at assigning robustness

ALGORITHM 1. Van Loan GRAPE algorithm.

Input: Target gate U_{tar} or state $\mathbf{r}_{\text{tar}}$
Lindblad operators $\{\mathbf{L}^{\alpha}, \mathbf{L}^{\beta}, \ldots, \mathbf{L}^{\gamma}\}$
Weighting coefficients $\{w^{n}_{\alpha,\beta,\ldots,\gamma}\}$
Set tolerance ϵ_0
Set step length χ
Output: Control parameters u_l^k
Initialization: Guess initial controls u_l^k
Evolution: $\Pi_{k=1}^{M} \exp\{\tau \mathbf{H}^k\}$
Cost function: $f(u) = -f_0(u) + f_1(u)$
while $f(u) \geqslant \epsilon_0$ **do**
  Calculate gradient $\frac{\partial f}{\partial u_l^k} = -\frac{\partial f_0}{\partial u_l^k} + \frac{\partial f_1}{\partial u_l^k}$
  Update: $u_l^k \leftarrow u_l^k - \chi \frac{\partial f}{\partial u_l^k}$
  Evolution: $\Pi_{k=1}^{M} \exp\{\tau \mathbf{H}^k\}$
  Cost function: $f(u) = -f_0(u) + f_1(u)$
end while

requirements, i.e.,

$$f_1(u) = \sum_{n} \sum_{\alpha,\beta,\ldots,\gamma} w^{n}_{\alpha,\beta,\ldots,\gamma} \left\| D_U^{(n)}(\mathbf{L}^{\alpha}, \mathbf{L}^{\beta}, \ldots, \mathbf{L}^{\gamma}) \right\|, \quad (19)$$

where $\|\cdot\|$ denotes the Frobenius norm, and $w^{n}_{\alpha,\beta,\ldots,\gamma}$ are some carefully chosen weighting coefficients. Overall, this is a multiobjective optimization problem, and the total cost function to be minimized can be expressed as

$$f(u) = -f_0(u) + f_1(u). \quad (20)$$

Various optimization algorithms can be chosen to optimize the control fields u for minimizing $f(u)$. Here, we employ the popular GRAPE algorithm [44]. Specifically, the overall evolution time T is divided into M equal steps, each with a duration of $\tau = T/M$ and a constant amplitude $u_l^k, k = 1, 2, \ldots, M$. The gradients of the cost function $f(u)$ with respect to u are analytically derived for updating the controls (see Appendix A for details). With employing the Van Loan integral formula to conveniently acquire directional derivatives within the GRAPE algorithm procedure, we refer to the overall algorithm as Van Loan GRAPE. The algorithmic pseudocode is presented in Algorithm 1.

III. QUANTUM STATE TRANSFER UNDER MARKOVIAN NOISE

In the following, we employ the introduced robust optimal control method to reduce the influence of Markovian noise in the context of quantum state transfer tasks.

A. Two-level system

We begin by considering the task of robust state transfer for two-level systems in the presence of Markovian noise. The Hamiltonian of a two-level quantum system in the interaction frame, with respect to the drive frequency ω_1, can be written as

$$H(t) = \frac{\delta}{2}\sigma_z + \frac{u_x(t)}{2}\sigma_x + \frac{u_y(t)}{2}\sigma_y, \quad (21)$$

where $\delta = \omega_0 - \omega_1$ denotes the detuning of the transition frequency ω_0 with respect to the drive frequency, σ_α ($\alpha = x, y, z$) represents Pauli matrix, and $u_x(t)$ and $u_y(t)$ are time-dependent transverse control fields. The unitary evolution part can be described using the Pauli basis within the Bloch representation, i.e.,

$$\mathbf{H}(t) = \begin{pmatrix} 0 & 0 & 0 & 0 \\ 0 & 0 & -\delta & u_y(t) \\ 0 & \delta & 0 & -u_x(t) \\ 0 & -u_y(t) & u_x(t) & 0 \end{pmatrix}. \quad (22)$$

Without loss of generality, we assume that the drive frequency is resonant with the transition frequency, i.e., $\delta = 0$. For the dissipative part, we consider the coexistence of amplitude damping and phase damping, thus their Lindblad operators read [54]

$$L_1 = \sigma_+ = \begin{pmatrix} 0 & 1 \\ 0 & 0 \end{pmatrix}, \quad L_2 = \sigma_z = \begin{pmatrix} 1 & 0 \\ 0 & -1 \end{pmatrix}. \quad (23)$$

As described above, these operators can be expressed in the Bloch representation, namely,

$$\mathbf{L}^1 = \begin{pmatrix} 0 & 0 & 0 & 0 \\ 0 & -\frac{1}{2} & 0 & 0 \\ 0 & 0 & -\frac{1}{2} & 0 \\ 1 & 0 & 0 & -1 \end{pmatrix},$$

$$\mathbf{L}^2 = \begin{pmatrix} 0 & 0 & 0 & 0 \\ 0 & -2 & 0 & 0 \\ 0 & 0 & -2 & 0 \\ 0 & 0 & 0 & 0 \end{pmatrix}. \quad (24)$$

By incorporating Eqs. (22) and (24) into Eq. (3), the system's evolution function is effectively established within the Bloch representation. We then follow the procedures introduced in Secs. II B and II C to search optimal controls for realizing robust state transfer under the considered Markovian noises.

As demonstration, we consider the problem of quantum state transfer from state polarized in the $-y$ direction ($\mathbf{r}_{-y} = [1/2, 0, -1/2, 0]$) to the y direction ($\mathbf{r}_y = [1/2, 0, 1/2, 0]$). By restricting the maximum Rabi frequency to $\Omega_{\max} = 50\times 2\pi$ MHz, a straightforward strategy is simply to apply a rectangular pulse along the x axis, with an amplitude of $\Omega_{\max}$ and a duration of $\pi/\Omega_{\max}$, i.e., $u_x(t) = \Omega_{\max}$, $u_y(t) = 0$, as depicted in Fig. 1(a). Using optimal control, the robust pulse found is depicted in Fig. 1(c), where we constrained $\sqrt{u_x^2(t) + u_y^2(t)} \leqslant \Omega_{\max}$ to ensure a fair comparison. It is evident that the optimal pulse corresponds to a π rotation along the $-x$ axis. To compare the robustness between these two pulses, we compute the state transfer fidelities for various values of the dissipative rates Γ_1 and Γ_2, as presented in Figs. 1(b) and 1(d). The significant enhancement in robustness against the two considered Markovian noises is clearly observed when employing our optimal pulse. Particularly, for amplitude damping quantified by Γ_1, our optimal pulse exhibits notably stronger robustness compared to the first pulse.

To understand the reason behind the improved robustness of our optimal pulse, we depict the evolution trajectories corresponding to these two pulses in the Bloch sphere for

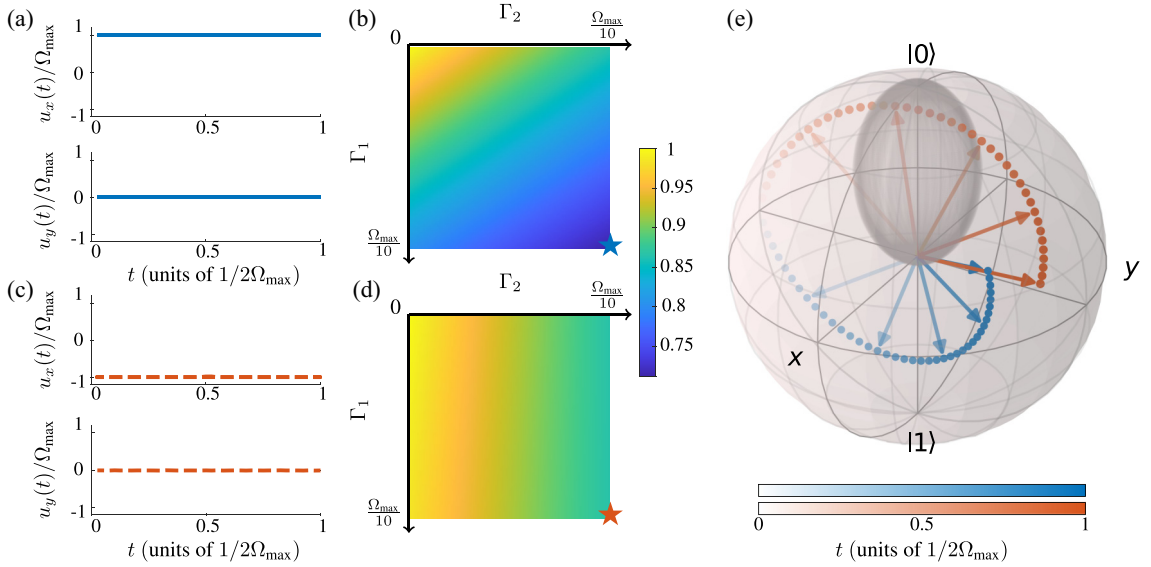

FIG. 1. Quantum state transfer from $\mathbf{r}_{-y} = [1/2, 0, -1/2, 0]$ to $\mathbf{r}_y = [1/2, 0, 1/2, 0]$ in a Markovian two-level system. (a), (c) demonstrate two π pulses that can implement perfect state transfer in the absence of noise, one rotating about the x axis, the other about the $-x$ axis. The considered Markovian noise can lead to different influences on these two evolution trajectories. Our algorithm yields the latter pulse with more robustness, thus demonstrating its ability to find the robust pulse. Here the number of optimized steps $M = 40$, and the maximal number of iterations is 80. (b), (d) show the state transfer fidelities in the presence of amplitude damping (Γ_1) and phase damping (Γ_2), which correspond to the evolution under pulses in (a) and (c), respectively. (e) plots their resulting evolution trajectories within the Bloch sphere. The gray ellipsoid is obtained according to Eq. (25) with $\Gamma_2 = 0$, within which the Markovian noise helps to recover the purity of quantum states.

$\Gamma_1 = \Gamma_2 = \Omega_{\max}/10$ [55]; see Fig. 1(e). While both the resultant final states are polarized along the target direction (y axis), the polarization of the state controlled by the first pulse (blue dots) decays more severely compared to that of the optimized one (red dots). This leads to a state transfer fidelity of 0.71, while using the optimized pulse we can improve to 0.87. The underlying reason can be explained through an analysis of the Markovian evolution under the control. We use the system purity function to study the impact from noise, which is defined as $p \equiv \mathrm{Tr}(\rho^2)$. For convenience, we express the quantum state as $\mathbf{r} = [1/2, x, y, z]^{\mathrm{T}}$ with $-1/2 \leqslant x, y, z \leqslant 1/2$. Thus, we have $p = 2\mathbf{r}^{\mathrm{T}}\mathbf{r}$, and its derivative with respect to time is $\dot{p} = 2(\dot{\mathbf{r}}^{\mathrm{T}}\mathbf{r} + \mathbf{r}^{\mathrm{T}}\dot{\mathbf{r}})$. By substituting Eq. (3) into $\dot{p} = 0$, we obtain

$$\left(\frac{\Gamma_1}{2} + 2\Gamma_2\right)(x^2 + y^2) - \Gamma_1\left(\frac{1}{2} - z\right)z = 0, \tag{25}$$

which forms an ellipsoid. This ellipsoid, as shown in the Bloch sphere in Fig. 1(e), clearly separates the Bloch sphere into two parts. For quantum states outside the ellipsoid, $\dot{p} < 0$, indicating that purity is about to decrease. Conversely, states inside the ellipsoid will gain purity. The intrinsic reason for the robustness of our Van Loan GRAPE method is that the evolved state under our optimized pulses traverses this ellipsoid, allowing it to recover some of the lost purity.

B. Three-level Λ system

Now, we apply our method to enhance the efficiency of state transfer in three-level Λ systems under the influence of Markovian noise. Specifically, we consider state transfer from the initially populated state $|0\rangle$ to the target state $|2\rangle$, as shown in Fig. 2(a). Usually, this is accomplished using the technique of stimulated Raman adiabatic passage (STIRAP) [56–59], which adiabatically transfers the population from $|0\rangle$ to $|2\rangle$ by coupling the intermediate state $|1\rangle$ through two pulsed fields: pump and Stokes. During STIRAP, the population becomes confined in a dark state created by the two-photon resonance between states $|0\rangle$ and $|2\rangle$, without involving the intermediate state $|1\rangle$ [60]. This is remarkable since it means that STIRAP is robust to the relaxation of state $|1\rangle$. However, its effectiveness is constrained due to the significant impact of decoherence on the timescale prescribed by the adiabatic theorem [61,62]. To address this problem, one can design shorter control pulses to achieve the wanted population transfer. However, in this scenario, the spontaneous emissions from the intermediate state will have noticeable impacts [60,63]. In the following, we describe how our robust optimal control method can design robust pulses to address this issue and compare it with two conventional schemes.

The system Hamiltonian and control Hamiltonian of a Λ system, considered in a frame rotating at both driving frequencies and under the rotating-wave approximation, are expressed as follows:

$$H_0 = \delta|1\rangle\langle 1| + \Delta|2\rangle\langle 2|, \tag{26}$$

$$H_C(t) = u_p(t)|0\rangle\langle 1| + u_s(t)|1\rangle\langle 2| + \mathrm{H.c.}, \tag{27}$$

where δ represents the one-photon detuning, Δ denotes the two-photon detuning, $u_p(t)$ is the pump pulse acting on the $|0\rangle \leftrightarrow |1\rangle$ transition, and $u_s(t)$ is the Stokes pulse on the $|1\rangle \leftrightarrow |2\rangle$ transition. Here, we let $\Delta = 0$ and only consider resonant STIRAP with one-photon detuning δ. The spontaneous emission from the intermediate state $|1\rangle$ can be characterized by

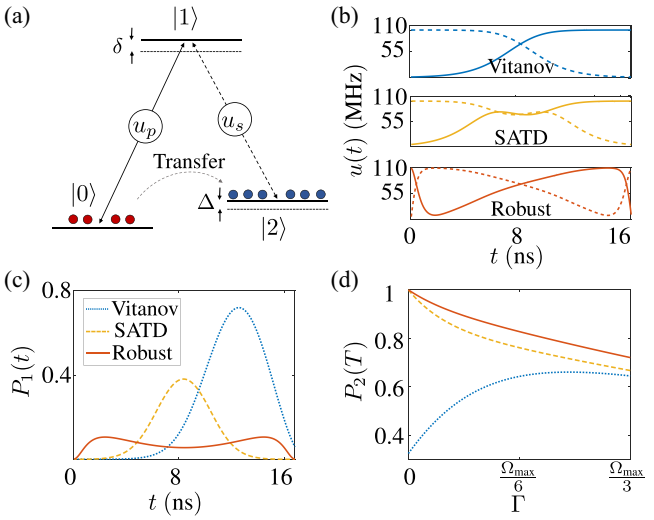

FIG. 2. Quantum state transfer in a Markovian three-level Λ system using STIRAP under different control schemes and the corresponding robustness. (a) Schematic diagram of STIRAP, where $|0\rangle$, $|1\rangle$, and $|2\rangle$ represent the initially populated, intermediate, and target states, respectively. Here, δ denotes the one-photon detuning, while Δ denotes the two-photon detuning. The terms $u_p(t)$ and $u_s(t)$ represent the pump and Stokes pulses, respectively. (b) Envelopes of the Vitanov pulses $u^{(1)}$, the SATD pulses $u^{(2)}$ and our robust pulses $u^{(3)}$, for realizing STIRAP, where solid lines denote the pump pulses $u_p(t)$, and dashed lines denote the Stokes pulses $u_s(t)$. Here the number of optimized steps $M = 200$, and the maximal number of iterations is 100. (c) The population on the intermediate state $|1\rangle$ during the evolution. (d) The final population on the target state for various spontaneous emission rates, where $\Gamma_1 = \Gamma_2 = \Gamma$.

the following Lindblad operators [60,64,65]

$$L_1 = |0\rangle\langle 1|, \quad L_2 = |2\rangle\langle 1|. \tag{28}$$

Expressing Eqs. (26) and (28) in the Bloch representation, and applying the procedures introduced in Secs. II B and II C, we can search robust pulses that can improve the effectiveness of STIRAP; see details in Appendix B.

For comparison, we first introduce a control scheme proposed in Ref. [66], which is known to be adiabatically optimal and robust to pulse variations as well as single-photon detuning. Precisely, the pulse shape, named as Vitanov pulse, is described by

$$u_s^{(1)}(t) = \Omega^{(1)}(t)\cos[\theta^{(1)}(t)], \tag{29}$$

$$u_p^{(1)}(t) = \Omega^{(1)}(t)\sin[\theta^{(1)}(t)], \tag{30}$$

with $\theta^{(1)}(t) = \pi/[2 + 2e^{-\nu(t-T/2)}]$ and $t \in [0, T]$. Here we set the parameters $\Omega^{(1)}(t) = 100\times 2\pi$ MHz, $\nu = 0.6$ GHz, and total pulse time $T = 16.8$ ns. As such, the adiabatic condition is not fully satisfied and the efficiency of STIRAP is limited even in the absence of dissipation. To speedup the adiabatic state transfer and minimize the occupancy of the intermediate level during evolution, there was proposed the superadiabatic transitionless driving (SATD) method for STIRAP [58,63]. It is constructed by modifying the Vitanov pulse to

$$u_s^{(2)}(t) = \Omega^{(2)}(t)\cos[\theta^{(2)}(t)], \tag{31}$$

$$u_p^{(2)}(t) = \Omega^{(2)}(t)\sin[\theta^{(2)}(t)], \tag{32}$$

where $\theta^{(2)}(t) = \theta^{(1)}(t) - \arctan[\dot{\xi}/\Omega^{(1)}(t)]$, $\Omega^{(2)}(t) = \sqrt{\Omega^{(1)}(t)^2 + \dot{\xi}^2}$, and $\xi = -\arctan[\dot{\theta}^{(1)}(t)/\Omega^{(1)}(t)]$. This restricts the evolution to a dressed state basis and facilitates rapid driving for the desired state transfer.

We demonstrate the pulse shapes of these three control schemes for STIRAP in Fig. 2(b). Our robust pulse, marked as $u_s^{(3)}$ and $u_p^{(3)}$, is found by minimizing the directional derivatives with respect to L_1 and L_2 up to the second order. For a fair comparison, we constrained the amplitude of $u^{(3)}$ not to exceed that of $u^{(2)}$, that is, $\max_t|u^{(3)}(t)| \leqslant \max_t|u^{(2)}(t)| \equiv \Omega_{\max}$ with $|u(t)| \equiv \sqrt{u_s^2(t) + u_p^2(t)}$ (see Appendix B for details). It is evident that the shapes of the Vitanov pulse ($u^{(1)}$) and the SATD pulse ($u^{(2)}$) are similar, while the shape of our robust pulse is different. To compare their performance on state transfer, we first display the variation of the population on the intermediate state during the evolution, i.e., $P_1(t) = \langle 1|\rho(t)|1\rangle$; see Fig. 2(c). For the Vitanov pulse, we observe that the population on the intermediate state remains small in the first half of the evolution but increases rapidly in the latter half, reaching up to 0.72. Meanwhile, the final $P_1(t)$ still has a residual value of 0.05. For the SATD pulse, $P_1(t)$ is symmetric and attains the maximum population of 0.38 in the middle time of the evolution, while at the final time it is negligible. With our robust pulse, the population on the intermediate state is maintained below 0.11 throughout the entire evolution process, and the final $P_1(t)$ is also negligible. From these results, we deduce that the efficiency of the state transfer can be considerably improved using our robust pulse. To verify this, we plot the final population on the target state, i.e., $P_2(T) \equiv \langle 2|\rho(T)|2\rangle$, under different values of spontaneous emission rates $\Gamma_1 = \Gamma_2 = \Gamma$; see Fig. 2(d). As expected, Vitanov pulse fail to achieve a high population on the target state even in the absence of spontaneous emission ($\Gamma = 0$). This is attributed to the relatively short evolution time, leading to the violation of the adiabatic theorem. Nevertheless, the significant occupation of the intermediate state contributes to the increase in $P_2(T)$ as the spontaneous emission rates rise, reaching up to 0.66 for $\Gamma = 0.24\Omega_{\max}$. SATD performs better due to its implementation of a fast adiabatic transfer strategy. Remarkably, our robust pulse outperforms both the Vitanov pulses, showcasing an improvement of $P_2(T)$ up to 0.68, and the SATD pulses, demonstrating an improvement of $P_2(T)$ up to 0.07, across the tested spontaneous emission rates.

IV. QUANTUM GATE UNDER MARKOVIAN NOISE

In this section, we investigate the application of our robust optimal control method to quantum gate preparation under Markovian noise.

A. Two-level system

We first consider preparing a NOT gate in a two-level system in the presence of both phase damping and amplitude damping. The system Hamiltonian and the Lindblad operators are Eqs. (22) and (23) as presented in Sec. III A. Following the procedures introduced in Secs. II B and II C, we can search optimal controls for realizing the target quantum gate under the considered Markovian noises.

During the optimization process, we limit the maximum Rabi frequency $\Omega_{\max}$ to not exceed $50\times 2\pi$ MHz, i.e., $\sqrt{u_x^2(t)+u_y^2(t)} \leqslant \Omega_{\max}$ and we set the duration of the control pulse as $T = 10$ ns. For the considered Markovian noises, we choose $\Gamma_1 = \Gamma_2 = \Omega_{\max}/10$. We divide the evolution into 40 discrete steps and set the maximal number of iterations as 80. For comparison, we employ the conventional GRAPE method without considering the robustness condition, and the gate fidelity reaches $f_{0,\text{gate}} = 86.52\%$. Applying our robust optimal control with Van Loan GRAPE, however, we find that the gate fidelity cannot be further improved, even with a longer pulse duration than T. This suggests that optimal control is not able to resist Markovian noise in a two-level system for the quantum gate problem.

B. Three-level ladder system

We then consider the task of preparing a NOT gate on the lowest two levels in a three-level ladder system subject to both phasing damping and amplitude damping. The motivation here is to see whether adding an extra level will make it possible to resist Markovian noises. As a concrete example, we investigate a superconducting transmon qubit, where the lowest two levels $|0\rangle$ and $|1\rangle$ serve as a qubit, and the third level $|2\rangle$ accounts for leakage; see Fig. 3(a). Working in a frame rotating at the drive frequency and employing the rotating wave approximation, the system's intrinsic Hamiltonian and the control Hamiltonian can be expressed as

$$H_0 = \delta|1\rangle\langle 1| + \Delta|2\rangle\langle 2|,$$
$$H_C(t) = \sum_{j=1,2}\left[\left(\frac{u_x(t)}{2} + i\frac{u_y(t)}{2}\right)\lambda_j|j\rangle\langle j-1| + \text{H.c.}\right],$$

where $u_{x,y}(t)$ couple the adjacent energy levels, the drive frequency is assumed to be resonant with the qubit frequency, i.e., $\delta = 0$, and Δ denotes the anharmonicity of the system. In our simulation, we set $\Delta = 400\times 2\pi$ MHz, $\lambda_1 = 1$, and $\lambda_2 = \sqrt{2}$, resulting in undesired leakage out of the qubit subspace. The Markovian noise we consider are amplitude damping and phasing damping, the corresponding Lindblad operators can be written as [67]

$$L_1 = |0\rangle\langle 1| + \sqrt{2}|1\rangle\langle 2|, \quad L_2 = \tfrac{2\sqrt{2}}{3}(|0\rangle\langle 0| - |2\rangle\langle 2|),$$
$$L_3 = \tfrac{\sqrt{2}}{3}(|0\rangle\langle 0| - |1\rangle\langle 1|), \quad L_4 = \tfrac{\sqrt{2}}{3}(|1\rangle\langle 1| - |2\rangle\langle 2|).$$

Following the procedures introduced in Secs. II B and II C, we can search for optimal controls to realize the target quantum gate under the considered Markovian noises.

During optimization, we restrict the maximum Rabi frequency to be $\Omega_{\max} = 500\times 2\pi$ MHz, and minimize the directional derivatives with respect to L_α ($\alpha = 1, 2, 3, 4$) up to the second order. For comparison, we also apply the conventional GRAPE algorithm to find pulses to implement the target NOT gate. Here, we set $\Gamma_1 = \Gamma_2 = \Gamma_3 = \Gamma_4 = \Omega_{\max}/10$. The initial guess for the optimal search is chosen as the first-order derivative removal by adiabatic gate (DRAG) pulse [46,68]. The corresponding pulse shapes are shown in Fig. 3(b). The gate fidelity using the pulse searched by the conventional GRAPE algorithm is 80.26%, which can be slightly improved to 80.29% with the pulse searched by our Van Loan GRAPE algorithm; see the dashed lines Fig. 3(d). To understand why our robust control can achieve enhancement, we plot the transition probability to the state $|2\rangle$ from $|0\rangle$ and $|1\rangle$ during the evolution, as depicted in Fig. 3(c). We observe a slight suppression of leakage to the state $|2\rangle$ during the evolution using our robust control compared to conventional GRAPE, implying an improved robustness to the considered noises. To further validate this result, we conduct 100 runs for both GRAPE algorithms with different randomly chosen initial values, as illustrated in Fig. 3(d). This bar plot reveals that the distribution of gate fidelities using our Van Loan GRAPE (red bars), with the standard deviation of 7.6×10^{-5}, is much narrower than that of the conventional GRAPE (blue bars), with the standard deviation of 2.8×10^{-4}. The mean gate fidelity is also slightly improved from 80.23% to 80.28%. This gives evidence suggesting that our Van Loan GRAPE may

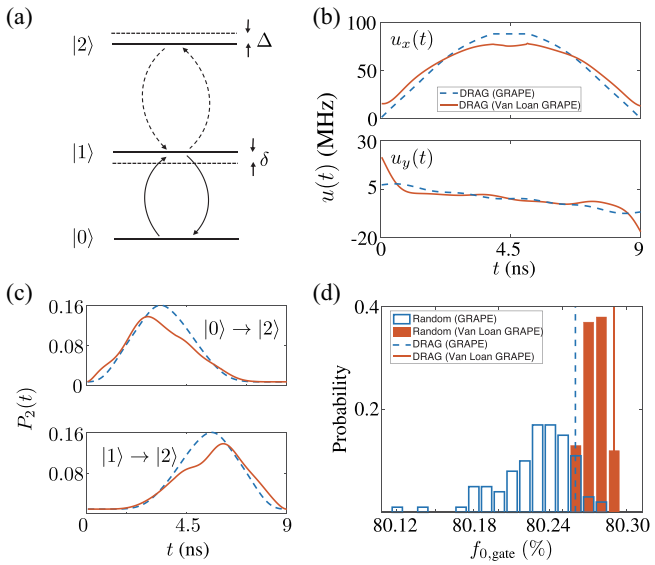

FIG. 3. Quantum gate in a Markovian three-level ladder system. (a) The qubit is formed by the states $|0\rangle$ and $|1\rangle$, while $|2\rangle$ accounts for leakage. The offset between the drive frequency and the qubit frequency is marked as δ, and Δ represents the anharmonicity of the system. (b) Control pulses searched by the conventional GRAPE algorithm and our Van Loan GRAPE algorithm. The initial guess is chosen as the DRAG pulse. Here the number of optimized steps $M = 200$, and the maximal number of iterations is 100. (c) Transition probability to $|2\rangle$ from $|0\rangle$ or $|1\rangle$ using pulses in (b), which are searched by the conventional GRAPE algorithm and our Van Loan GRAPE algorithm. (d) Statistical distribution of quantum gate fidelities for 100 runs with different random initial controls. The dashed lines indicate the results obtained with the initial guess of the DRAG pulse.

more easily improve gate fidelity under the considered Markovian noise. The current scenario differs from the previously discussed two-level case, primarily due to the presence of an additional energy level $|2\rangle$ in the system, which introduces possibilities for robust optimal control to drive the system within subspaces characterized by low dissipative rates. Compared with optimizing a specific evolution trajectory for the problem of quantum state transfer, the task of quantum gate is more restrictive as it requires resisting relaxation over the entire state space. Due to the inevitable transition into the state $|2\rangle$ and the existence of dissipation, though slower, between $|0\rangle$ and $|1\rangle$, the performance of quantum gate can only be slightly improved. This result is consistent with previous studies [25,28].

V. SUMMARY AND DISCUSSIONS

Although numerous effective methods have been developed to suppress quasistatic and slowly varying noises in routine control tasks, the resistance of fast fluctuating Markovian noise remains a challenging and less explored problem. Our work presents a robust quantum optimal control method for tackling Markovian noises described by Lindblad operators. The numerical simulations of quantum state transfer in a two-level system and a three-level Λ system demonstrate that our method can significantly enhance fidelity compared to conventional control strategies, including the mentioned two STIRAP pulses. In the context of quantum gate preparation under Markovian noise, the numerical results indicate that the gate fidelity cannot be improved for a two-level system and can only be slightly enhanced for a three-level ladder system; this agrees with findings from previous studies [25,28].

The current work presents a practical and versatile method for addressing Markovian noises, extendable to other control scenarios such as quantum sensing [69,70] and quantum information processing [71]. Moreover, our method is applicable for tackling Markovian noises in multilevel and multiqubit systems, where the increasing complexity of noises and parameter spaces offer additional opportunities for optimization [72]. To alleviate the exponentially increasing computational cost, we can further incorporate the hybrid quantum-classical approach [73] and variational quantum algorithms [74] into our robust control protocol. Additionally, our approach can be further enhanced by introducing ancillary qubits to provide more optimization spaces and additional incoherent operations to potentially recover the noisy dynamics [75]. While the number of examples demonstrating successful control of Markovian quantum systems is increasing, our current comprehension of controllability and the most promising control strategies for Markovian quantum systems remains relatively restricted. Thus the design of advanced suppression methods may necessitate resorting to relevant theoretical studies, such as quantum speed limit [76,77] and controllability analysis [40].

ACKNOWLEDGMENTS

This work was supported by the National Natural Science Foundation of China (Grants No. 12204230 and No. 12122506), Shenzhen Science and Technology Program (Grants No. RCYX20200714114522109 and No. KQTD20200820113010023), Guangdong Basic and Applied Basic Research Foundation (Grant No. 2021B1515020070), and Postdoctoral Fellowship Program of CPSF (Grant No. GZC20231727).

APPENDIX A: GRADIENT OF COST FUNCTION

The cost function f is the weighted sum of fidelity and the magnitudes of the directional derivatives, as mentioned in Eq. (20), and the goal is to find the optimal control that minimizes f. The gradient of f with respect to each piecewise control field is needed for the gradient-based algorithm, which can also be expressed as the weighted sum of the gradient of fidelity and directional derivatives, i.e.,

$$\frac{\partial f}{\partial u_l^k} = -\frac{\partial f_0}{\partial u_l^k} + \frac{\partial f_1}{\partial u_l^k}. \tag{A1}$$

In the following, we show the detailed calculations.

We first calculate $\partial f_0/\partial u_l^k$. Let $\mathbf{H}^k = \mathbf{H}_S + \sum_l u_l^k \mathbf{H}_C^l$ denotes $H_S + \sum_l u_l^k H_C^l$ in the Bloch representation. Due to the discretization of the total evolution, the only term contains u_l^k is the evolution at the kth step, i.e., $e^{\Delta t \mathbf{H}^k}$. Hence

$$\frac{f_{0,\text{state}}}{u_l^k} = \mathbf{r}_{\text{tar}}^{\text{T}}\left[\left(\Pi_{m=k+1}^{M} e^{\Delta t \mathbf{H}^m}\right)\frac{\partial e^{\Delta t \mathbf{H}^k}}{\partial u_l^k}\left(\Pi_{m=1}^{k-1} e^{\Delta t \mathbf{H}^m}\right)\right]\mathbf{r}_0.$$

According to the standard formula $\partial_x e^{A(x)} = \int_0^1 e^{\tau A}(\partial_x A) e^{(1-\tau)A} d\tau$, we have

$$\begin{aligned}\frac{\partial e^{\Delta t \mathbf{H}^k}}{\partial u_l^k} &= \Delta t \int_0^1 e^{\tau \Delta t \mathbf{H}^k}\left(\frac{\partial \mathbf{H}^k}{\partial u_l^k}\right) e^{-\tau \Delta t \mathbf{H}^k} d\tau e^{\Delta t \mathbf{H}^k} \\ &= \Delta t \int_0^1 e^{\tau \Delta t \mathbf{H}^k} \mathbf{H}_C^l e^{-\tau \Delta t \mathbf{H}^k} d\tau e^{\Delta t \mathbf{H}^k}. \\ &= \Delta t \int_0^1 e^{\tau \Delta t \mathbf{H}^{k,\times}} \mathbf{H}_C^l d\tau e^{\Delta t \mathbf{H}^k},\end{aligned} \tag{A2}$$

with $\mathbf{H}^{k,\times}$ being the commutation superoperator, i.e., $A^{\times}B = [A, B]$. This expression can be further expanded with the Taylor series

$$\begin{aligned}\frac{\partial e^{\Delta t \mathbf{H}^k}}{\partial u_l^k} &= \Delta t \int_0^1 \sum_{n=0}^{\infty} \frac{(\tau \Delta t)^n d\tau}{n!} (\mathbf{H}^{k,\times})^n \mathbf{H}_C^l e^{\Delta t \mathbf{H}^k} \\ &= \sum_{n=0}^{\infty} \frac{(\Delta t)^{n+1}}{(n+1)!} (\mathbf{H}^{k,\times})^n \mathbf{H}_C^l e^{\Delta t \mathbf{H}^k}.\end{aligned} \tag{A3}$$

Gradients with arbitrary-order accuracy can thus be evaluated from a finite sum of commutators. Here we assume the condition $\Delta t \ll \|\mathbf{H}^k\|^{-1}$ is satisfied. Using the first order in Δt, Eq. (A3) becomes $\Delta t \mathbf{H}_C^l e^{\Delta t \mathbf{H}^k}$. Denote the shorthand notation $V_k^j = \prod_{m=k}^{j} e^{\Delta t \mathbf{H}^m}$, then the gradient of fidelity to the first order in Δt is

$$\frac{\partial f_{0,\text{state}}}{\partial u_l^k} = (\Delta t)\mathbf{r}_{\text{tar}}^{\text{T}}\left[V_{k+1}^M \mathbf{H}_C^l V_1^k\right]\mathbf{r}_0.$$

Similarly,

$$\frac{\partial f_{0,\text{gate}}}{\partial u_l^k} = \frac{\Delta t}{6}\sum_j (U_{\text{tar}}\mathbf{r}_j)^{\text{T}}\left[V_{k+1}^M \mathbf{H}_C^l V_1^k\right]\mathbf{r}_0.$$

For the first-order gradient of directional derivatives, the technique of Van Loan integral formula is used again

$$\frac{\partial f_1}{\partial u_l^k} = 2\sum_n \sum_{\alpha,\beta,\ldots\gamma} w^n_{\alpha,\beta,\ldots\gamma} \times \mathrm{Re}\Big[\big(\Pi_{m=1}^{M} e^{\Delta t \mathcal{G}^m}\big)^{\dagger}_{1,n+1} \times \big(\Pi_{m=k+1}^{M} e^{\Delta t \mathcal{G}^m} \mathcal{G}_C^l \Pi_{m=1}^{k} e^{\Delta t \mathcal{G}^m}\big)_{1,n+1}\Big], \tag{A4}$$

with

$$\mathcal{G}^m = \begin{pmatrix} \mathbf{H}^m & \mathbf{L}^\alpha & 0 & \ldots & 0 \\ 0 & \mathbf{H}^m & \mathbf{L}^\beta & \ldots & 0 \\ \vdots & \vdots & \vdots & \ddots & \vdots \\ 0 & 0 & 0 & \ldots & \mathbf{L}^\gamma \\ 0 & 0 & 0 & \ldots & \mathbf{H}^m \end{pmatrix}, \tag{A5}$$

and

$$\mathcal{G}_C^l = \begin{pmatrix} \mathbf{H}_C^l & \mathbf{L}^\alpha & 0 & \ldots & 0 \\ 0 & \mathbf{H}_C^l & \mathbf{L}^\beta & \ldots & 0 \\ \vdots & \vdots & \vdots & \ddots & \vdots \\ 0 & 0 & 0 & \ldots & \mathbf{L}^\gamma \\ 0 & 0 & 0 & \ldots & \mathbf{H}_C^l \end{pmatrix}. \tag{A6}$$

APPENDIX B: DETAILS OF ROBUST STIRAP

For the three-level quantum system, we work in the Bloch representation by expanding the state and the operators with respect to the traceless Hermitian Gell-Mann matrices of the SU(3) group, i.e.,

$$\lambda_1 = \begin{pmatrix} 0 & 1 & 0 \\ 1 & 0 & 0 \\ 0 & 0 & 0 \end{pmatrix}, \quad \lambda_2 = \begin{pmatrix} 0 & -i & 0 \\ i & 0 & 0 \\ 0 & 0 & 0 \end{pmatrix},$$
$$\lambda_3 = \begin{pmatrix} 1 & 0 & 0 \\ 0 & -1 & 0 \\ 0 & 0 & 0 \end{pmatrix}, \quad \lambda_4 = \begin{pmatrix} 0 & 0 & 1 \\ 0 & 0 & 0 \\ 1 & 0 & 0 \end{pmatrix},$$
$$\lambda_5 = \begin{pmatrix} 0 & 0 & -i \\ 0 & 0 & 0 \\ i & 0 & 0 \end{pmatrix}, \quad \lambda_6 = \begin{pmatrix} 0 & 0 & 0 \\ 0 & 0 & 1 \\ 0 & 1 & 0 \end{pmatrix},$$
$$\lambda_7 = \begin{pmatrix} 0 & 0 & 0 \\ 0 & 0 & -i \\ 0 & i & 0 \end{pmatrix}, \quad \lambda_8 = \frac{1}{\sqrt{3}} \begin{pmatrix} 1 & 0 & 0 \\ 0 & 1 & 0 \\ 0 & 0 & -2 \end{pmatrix}.$$

These matrices obey the trace orthonormality relation. In this way, we work in a real representation, which is convenient for numerical computations.

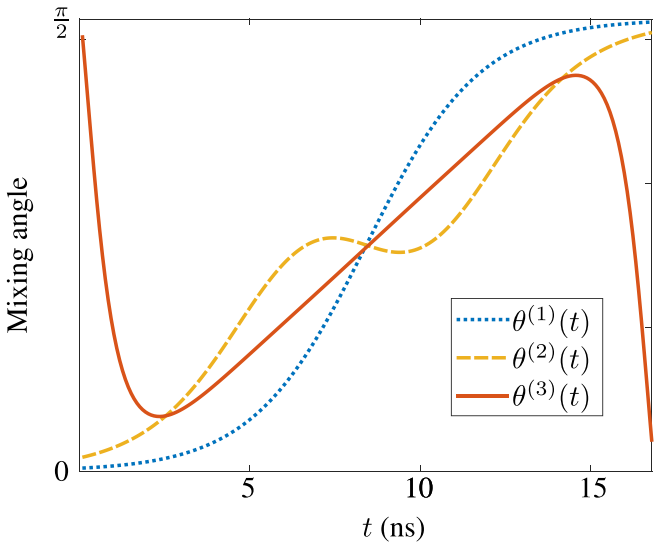

FIG. 4. Mixing angles of STIRAPs under different control strategies. $\theta^{(1)}(t)$, $\theta^{(2)}(t)$, and $\theta^{(3)}(t)$ correspond to the mixing angles of the Vitanov pulse, SATD pulse and our robust pulse, respectively.

We then compare the performance of our Van Loan GRAPE with the SATD given by Eq. (31). For a fair comparison, we limit the amplitude of searched control fields $\max_t |u^{(3)}(t)| \leqslant \max_t |u^{(2)}(t)|$ with $|u(t)| \equiv \sqrt{u_s^2(t) + u_p^2(t)}$. To this end, we change the form of control field as

$$u_p(t)|0\rangle\langle 1| + u_s(t)|1\rangle\langle 2| + \mathrm{H.c.}$$
$$\to \Omega_{\max}\big[\sin(\theta^{(3)}(t))|0\rangle\langle 1| + \cos(\theta^{(3)}(t))|1\rangle\langle 2| + \mathrm{H.c.}\big],$$

with $\Omega_{\max} = \max_t |u^{(2)}(t)|$, and the only parameter to optimize is the mixing angle $\theta^{(3)}(t)$. To employ the Van Loan GRAPE algorithm, we calculate the gradient of fidelity via the chain rule for derivatives

$$\frac{\partial f_{0,\mathrm{state}}}{\partial \theta_k^{(3)}} = (\Omega_{\max}\Delta t)\mathbf{r}_{\mathrm{tar}}^{\mathrm{T}}\Big[\big(\Pi_{m=k+1}^{M} e^{\Delta t \mathbf{H}^m}\big) \times \big[\cos\big(\theta_k^{(3)}\big)\mathbf{H}^p - \sin\big(\theta_k^{(3)}\big)\mathbf{H}^s\big]\big(\Pi_{m=1}^{k} e^{\Delta t \mathbf{H}^m}\big)\Big]\mathbf{r}_0. \tag{B1}$$

with $\mathbf{H}^p, \mathbf{H}^s$ being $|0\rangle\langle 1| + \mathrm{H.c.}$, $|1\rangle\langle 2| + \mathrm{H.c.}$ in the Bloch representation. The gradient of f_2 can be given in a similar way.

The mixing angles in our simulation, which is closely related to the population on the target state $|3\rangle$ in the STIRAP, is shown in Fig. 4. For the adiabatic evolution and SATD, the conditions of $\theta(t=0) = 0$ and $\theta(t=T) = \pi/2$ are satisfied, thus in line with the standard design of STIRAP [45]. The mixing angle optimized via Van Loan GRAPE oscillates, and the behaviors at $t = 0$ and $t = T$ are also significantly different with previous designs.

[1] D. Suter and G. A. Álvarez, *Colloquium:* Protecting quantum information against environmental noise, Rev. Mod. Phys. **88**, 041001 (2016).

[2] M. H. Levitt, Composite pulses, Prog. Nucl. Magn. Reson. Spectrosc. **18**, 61 (1986).

[3] X. Wang, L. S. Bishop, J. Kestner, E. Barnes, K. Sun, and S. Das Sarma, Composite pulses for robust universal control of singlet–triplet qubits, Nat. Commun. **3**, 997 (2012).

[4] A. D. Leu, M. F. Gely, M. A. Weber, M. C. Smith, D. P. Nadlinger, and D. M. Lucas, Fast, high-fidelity addressed

single-qubit gates using efficient composite pulse sequences, Phys. Rev. Lett. **131**, 120601 (2023).
[5] T. Nöbauer, A. Angerer, B. Bartels, M. Trupke, S. Rotter, J. Schmiedmayer, F. Mintert, and J. Majer, Smooth optimal quantum control for robust solid-state spin magnetometry, Phys. Rev. Lett. **115**, 190801 (2015).
[6] G. Dridi, K. Liu, and S. Guérin, Optimal robust quantum control by inverse geometric optimization, Phys. Rev. Lett. **125**, 250403 (2020).
[7] J. C. Saywell, M. S. Carey, P. S. Light, S. S. Szigeti, A. R. Milne, K. S. Gill, M. L. Goh, V. S. Perunicic, N. M. Wilson, C. D. Macrae, A. Rischka, P. J. Everitt, N. P. Robins, R. P. Anderson, M. R. Hush, and M. J. Biercuk, Enhancing the sensitivity of atom-interferometric inertial sensors using robust control, Nat. Commun. **14**, 7626 (2023).
[8] M. Harutyunyan, F. Holweck, D. Sugny, and S. Guérin, Digital optimal robust control, Phys. Rev. Lett. **131**, 200801 (2023).
[9] W. D. Oliver, Engineering a revolution, Nat. Phys. **10**, 794 (2014).
[10] J. Bylander, S. Gustavsson, F. Yan, F. Yoshihara, K. Harrabi, G. Fitch, D. G. Cory, Y. Nakamura, J.-S. Tsai, and W. D. Oliver, Noise spectroscopy through dynamical decoupling with a superconducting flux qubit, Nat. Phys. **7**, 565 (2011).
[11] D. M. Tennant, L. A. Martinez, K. M. Beck, S. R. O'Kelley, C. D. Wilen, R. McDermott, J. L. DuBois, and Y. J. Rosen, Low-frequency correlated charge-noise measurements across multiple energy transitions in a tantalum transmon, PRX Quantum **3**, 030307 (2022).
[12] O. E. Dial, M. D. Shulman, S. P. Harvey, H. Bluhm, V. Umansky, and A. Yacoby, Charge noise spectroscopy using coherent exchange oscillations in a singlet-triplet qubit, Phys. Rev. Lett. **110**, 146804 (2013).
[13] N. Bar-Gill, L. M. Pham, C. Belthangady, D. Le Sage, P. Cappellaro, J. Maze, M. D. Lukin, A. Yacoby, and R. Walsworth, Suppression of spin-bath dynamics for improved coherence of multi-spin-qubit systems, Nat. Commun. **3**, 858 (2012).
[14] M. Kang, Y. Wang, C. Fang, B. Zhang, O. Khosravani, J. Kim, and K. R. Brown, Designing filter functions of frequency-modulated pulses for high-fidelity two-qubit gates in ion chains, Phys. Rev. Appl. **19**, 014014 (2023).
[15] A. R. Milne, C. L. Edmunds, C. Hempel, F. Roy, S. Mavadia, and M. J. Biercuk, Phase-modulated entangling gates robust to static and time-varying errors, Phys. Rev. Appl. **13**, 024022 (2020).
[16] L. Viola, E. Knill, and S. Lloyd, Dynamical decoupling of open quantum systems, Phys. Rev. Lett. **82**, 2417 (1999).
[17] C. A. Ryan, J. S. Hodges, and D. G. Cory, Robust decoupling techniques to extend quantum coherence in diamond, Phys. Rev. Lett. **105**, 200402 (2010).
[18] R. Rizzato, M. Schalk, S. Mohr, J. C. Hermann, J. P. Leibold, F. Bruckmaier, G. Salvitti, C. Qian, P. Ji, G. V. Astakhov *et al.*, Extending the coherence of spin defects in hbn enables advanced qubit control and quantum sensing, Nat. Commun. **14**, 5089 (2023).
[19] J. M. Martinis, S. Nam, J. Aumentado, K. M. Lang, and C. Urbina, Decoherence of a superconducting qubit due to bias noise, Phys. Rev. B **67**, 094510 (2003).
[20] F. Poggiali, P. Cappellaro, and N. Fabbri, Optimal control for one-qubit quantum sensing, Phys. Rev. X **8**, 021059 (2018).
[21] P. Cerfontaine, T. Hangleiter, and H. Bluhm, Filter functions for quantum processes under correlated noise, Phys. Rev. Lett. **127**, 170403 (2021).
[22] C. P. Koch, Controlling open quantum systems: Tools, achievements, and limitations, J. Phys.: Condens. Matter **28**, 213001 (2016).
[23] G. Lindblad, On the generators of quantum dynamical semigroups, Commun. Math. Phys. **48**, 119 (1976).
[24] D. Manzano, A short introduction to the lindblad master equation, AIP Adv. **10**, 025106 (2020).
[25] F. F. Floether, P. de Fouquieres, and S. G. Schirmer, Robust quantum gates for open systems via optimal control: Markovian versus non-Markovian dynamics, New J. Phys. **14**, 073023 (2012).
[26] C. Altafini, Controllability properties for finite dimensional quantum Markovian master equations, J. Math. Phys. **44**, 2357 (2003).
[27] N. Khaneja, T. Reiss, B. Luy, and S. J. Glaser, Optimal control of spin dynamics in the presence of relaxation, J. Magn. Reson. **162**, 311 (2003).
[28] T. Schulte-Herbrüggen, A. Spörl, N. Khaneja, and S. J. Glaser, Optimal control for generating quantum gates in open dissipative systems, J. Phys. B: At. Mol. Opt. Phys. **44**, 154013 (2011).
[29] J. Jing, L.-A. Wu, M. S. Sarandy, and J. G. Muga, Inverse engineering control in open quantum systems, Phys. Rev. A **88**, 053422 (2013).
[30] J. Liu and H. Yuan, Quantum parameter estimation with optimal control, Phys. Rev. A **96**, 012117 (2017).
[31] Y. Zhai, X. Yang, K. Tang, X. Long, X. Nie, T. Xin, D. Lu, and J. Li, Control-enhanced quantum metrology under Markovian noise, Phys. Rev. A **107**, 022602 (2023).
[32] E. Knill, R. Laflamme, and L. Viola, Theory of quantum error correction for general noise, Phys. Rev. Lett. **84**, 2525 (2000).
[33] S. J. Beale, J. J. Wallman, M. Gutiérrez, K. R. Brown, and R. Laflamme, Quantum error correction decoheres noise, Phys. Rev. Lett. **121**, 190501 (2018).
[34] S. Zhou, M. Zhang, J. Preskill, and L. Jiang, Achieving the Heisenberg limit in quantum metrology using quantum error correction, Nat. Commun. **9**, 78 (2018).
[35] D. A. Lidar, I. L. Chuang, and K. B. Whaley, Decoherence-free subspaces for quantum computation, Phys. Rev. Lett. **81**, 2594 (1998).
[36] T. Monz, K. Kim, A. S. Villar, P. Schindler, M. Chwalla, M. Riebe, C. F. Roos, H. Häffner, W. Hänsel, M. Hennrich, and R. Blatt, Realization of universal ion-trap quantum computation with decoherence-free qubits, Phys. Rev. Lett. **103**, 200503 (2009).
[37] Z. Zhu, T. Chen, X. Yang, J. Bian, Z.-Y. Xue, and X. Peng, Single-loop and composite-loop realization of nonadiabatic holonomic quantum gates in a decoherence-free subspace, Phys. Rev. Appl. **12**, 024024 (2019).
[38] C. Altafini, Coherent control of open quantum dynamical systems, Phys. Rev. A **70**, 062321 (2004).
[39] G. Dirr, U. Helmke, I. Kurniawan, and T. Schulte-Herbrüggen, Lie-semigroup structures for reachability and control of open quantum systems: Kossakowski-Lindblad generators form lie wedge to Markovian channels, Rep. Math. Phys. **64**, 93 (2009).
[40] J. Li, D. Lu, Z. Luo, R. Laflamme, X. Peng, and J. Du, Approximation of reachable sets for coherently controlled open

quantum systems: Application to quantum state engineering, Phys. Rev. A **94**, 012312 (2016).
[41] K. Kobayashi and N. Yamamoto, Control limit on quantum state preparation under decoherence, Phys. Rev. A **99**, 052347 (2019).
[42] H. Haas, D. Puzzuoli, F. Zhang, and D. G. Cory, Engineering effective Hamiltonians, New J. Phys. **21**, 103011 (2019).
[43] C. Van Loan, Computing integrals involving the matrix exponential, IEEE Trans. Automat. Contr. **23**, 395 (1978).
[44] N. Khaneja, T. Reiss, C. Kehlet, T. Schulte-Herbrüggen, and S. J. Glaser, Optimal control of coupled spin dynamics: design of NMR pulse sequences by gradient ascent algorithms, J. Magn. Reson. **172**, 296 (2005).
[45] N. V. Vitanov, A. A. Rangelov, B. W. Shore, and K. Bergmann, Stimulated Raman adiabatic passage in physics, chemistry, and beyond, Rev. Mod. Phys. **89**, 015006 (2017).
[46] F. Motzoi, J. M. Gambetta, P. Rebentrost, and F. K. Wilhelm, Simple pulses for elimination of leakage in weakly nonlinear qubits, Phys. Rev. Lett. **103**, 110501 (2009).
[47] H.-P. Breuer, E.-M. Laine, J. Piilo, and B. Vacchini, *Colloquium:* Non-Markovian dynamics in open quantum systems, Rev. Mod. Phys. **88**, 021002 (2016).
[48] B.-H. Liu, L. Li, Y.-F. Huang, C.-F. Li, G.-C. Guo, E.-M. Laine, H.-P. Breuer, and J. Piilo, Experimental control of the transition from Markovian to non-Markovian dynamics of open quantum systems, Nat. Phys. **7**, 931 (2011).
[49] X. Wang and S. G. Schirmer, Contractivity of the Hilbert-Schmidt distance under open-system dynamics, Phys. Rev. A **79**, 052326 (2009).
[50] F. J. Dyson, The radiation theories of Tomonaga, Schwinger, and Feynman, Phys. Rev. **75**, 486 (1949).
[51] D. Daems, A. Ruschhaupt, D. Sugny, and S. Guérin, Robust quantum control by a single-shot shaped pulse, Phys. Rev. Lett. **111**, 050404 (2013).
[52] M. A. Nielsen, A simple formula for the average gate fidelity of a quantum dynamical operation, Phys. Lett. A **303**, 249 (2002).
[53] M. D. Bowdrey, D. K. L. Oi, A. Short, K. Banaszek, and J. Jones, Fidelity of single qubit maps, Phys. Lett. A **294**, 258 (2002).
[54] M. A. Nielsen and I. L. Chuang, *Quantum Computation and Quantum Information* (Cambridge University Press, Cambridge, England, 2010).
[55] J. R. Johansson, P. D. Nation, and F. Nori, QUTIP: An open-source python framework for the dynamics of open quantum systems, Comput. Phys. Commun. **183**, 1760 (2012).
[56] Y.-X. Du, Z.-T. Liang, Y.-C. Li, X.-X. Yue, Q.-X. Lv, W. Huang, X. Chen, H. Yan, and S.-L. Zhu, Experimental realization of stimulated Raman shortcut-to-adiabatic passage with cold atoms, Nat. Commun. **7**, 12479 (2016).
[57] K. S. Kumar, A. Vepsäläinen, S. Danilin, and G. S. Paraoanu, Stimulated Raman adiabatic passage in a three-level superconducting circuit, Nat. Commun. **7**, 10628 (2016).
[58] A. Baksic, H. Ribeiro, and A. A. Clerk, Speeding up adiabatic quantum state transfer by using dressed states, Phys. Rev. Lett. **116**, 230503 (2016).
[59] F. J. González and R. Coto, Decoherence-protected quantum register of nuclear spins in diamond, Quantum Sci. Technol. **7**, 025015 (2022).
[60] P. A. Ivanov, N. V. Vitanov, and K. Bergmann, Spontaneous emission in stimulated Raman adiabatic passage, Phys. Rev. A **72**, 053412 (2005).
[61] Q. Shi and E. Geva, Stimulated Raman adiabatic passage in the presence of dephasing, J. Chem. Phys. **119**, 11773 (2003).
[62] P. A. Ivanov, N. V. Vitanov, and K. Bergmann, Effect of dephasing on stimulated Raman adiabatic passage, Phys. Rev. A **70**, 063409 (2004).
[63] B. B. Zhou, A. Baksic, H. Ribeiro, C. G. Yale, F. J. Heremans, P. C. Jerger, A. Auer, G. Burkard, A. A. Clerk, and D. D. Awschalom, Accelerated quantum control using superadiabatic dynamics in a solid-state lambda system, Nat. Phys. **13**, 330 (2017).
[64] M. Scala, B. Militello, A. Messina, and N. V. Vitanov, Stimulated Raman adiabatic passage in an open quantum system: Master equation approach, Phys. Rev. A **81**, 053847 (2010).
[65] M. Scala, B. Militello, A. Messina, and N. V. Vitanov, Microscopic description of dissipative dynamics of a level-crossing transition, Phys. Rev. A **84**, 023416 (2011).
[66] G. S. Vasilev, A. Kuhn, and N. V. Vitanov, Optimum pulse shapes for stimulated Raman adiabatic passage, Phys. Rev. A **80**, 013417 (2009).
[67] B. M. Varbanov, F. Battistel, B. M. Tarasinski, V. P. Ostroukh, T. E. O'Brien, L. DiCarlo, and B. M. Terhal, Leakage detection for a transmon-based surface code, npj Quantum Inf. **6**, 102 (2020).
[68] Z. Chen, J. Kelly, C. Quintana, R. Barends, B. Campbell, Y. Chen, B. Chiaro, A. Dunsworth, A. G. Fowler, E. Lucero, E. Jeffrey, A. Megrant, J. Mutus, M. Neeley, C. Neill, P. J. J. O'Malley, P. Roushan, D. Sank, A. Vainsencher, J. Wenner *et al.*, Measuring and suppressing quantum state leakage in a superconducting qubit, Phys. Rev. Lett. **116**, 020501 (2016).
[69] X. Yang, Y. Ge, B. Zhang, and J. Li, Robust dynamical decoupling for the manipulation of a spin network via a single spin, Phys. Rev. Appl. **18**, 054075 (2022).
[70] Y. Zhang, H. Wu, X. Yang, T. Xie, Y.-X. Wang, C. Liu, Q. Zhao, J. Ma, J. Li, and B. Zhang, Robust quantum control for the manipulation of solid-state spins, Phys. Rev. Appl. **19**, 034068 (2023).
[71] F. Verstraete, M. M. Wolf, and J. Ignacio Cirac, Quantum computation and quantum-state engineering driven by dissipation, Nat. Phys. **5**, 633 (2009).
[72] J. Li, R. Fan, H. Wang, B. Ye, B. Zeng, H. Zhai, X. Peng, and J. Du, Measuring out-of-time-order correlators on a nuclear magnetic resonance quantum simulator, Phys. Rev. X **7**, 031011 (2017).
[73] J. Li, X. Yang, X. Peng, and C.-P. Sun, Hybrid quantum-classical approach to quantum optimal control, Phys. Rev. Lett. **118**, 150503 (2017).
[74] K. Bharti, A. Cervera-Lierta, T. H. Kyaw, T. Haug, S. Alperin-Lea, A. Anand, M. Degroote, H. Heimonen, J. S. Kottmann, T. Menke, W.-K. Mok, S. Sim, L.-C. Kwek, and A. Aspuru-Guzik, Noisy intermediate-scale quantum algorithms, Rev. Mod. Phys. **94**, 015004 (2022).
[75] H. Kwon, R. Mukherjee, and M. S. Kim, Reversing Lindblad dynamics via continuous Petz recovery map, Phys. Rev. Lett. **128**, 020403 (2022).

[76] S. S. Hegde, J. Zhang, and D. Suter, Toward the speed limit of high-fidelity two-qubit gates, Phys. Rev. Lett. **128**, 230502 (2022).

[77] V. Negîrneac, H. Ali, N. Muthusubramanian, F. Battistel, R. Sagastizabal, M. S. Moreira, J. F. Marques, W. J. Vlothuizen, M. Beekman, C. Zachariadis, N. Haider, A. Bruno, and L. DiCarlo, High-fidelity controlled-z gate with maximal intermediate leakage operating at the speed limit in a superconducting quantum processor, Phys. Rev. Lett. **126**, 220502 (2021).